Ain Shams Engineering Journal 13 (2022) 101655

Contents lists available at ScienceDirect

Ain Shams Engineering Journal

journal homepage: www.sciencedirect.com

Performance enhancement and power management strategy of an autonomous hybrid fuel cell/wind power system based on adaptive neuro fuzzy inference system

Shiref A. Abdalla [a,*], Shahrum S. Abdullah [a], Ahmed M. Kassem [b]

[a] Malaysia-Japan International Institute of Technology (MJIIT), UTM Kuala Lumpur, Jalan Sultan Yahya Petra, Kuala Lumpur 54100, Malaysia
[b] Electrical Engineering Dept., Faculty of Engineering, Sohag University, Sohag, Egypt

ARTICLE INFO

Article history:
Received 4 June 2021
Revised 13 November 2021
Accepted 26 November 2021
Available online 13 December 2021

Keywords:
ANFIS
Fuel cell
Fuzzy logic
PMSG
IM
Renewable power generation
Wind power

ABSTRACT

In this paper, a hybrid wind/fuel cell generation system which can be used for loads in remote areas as a micro grid application is considered. This micro grid mainly includes fuel cell (FC), wind generator as electrical power suppliers, resistive-inductive impedance as static load, induction motor (IM) as a dynamic load, DC/AC converter and water electrolizer for supplying hydrogen gas. The Fuel cell is used to compensate the decrease in the power generated by wind, which leads to an increase in the system efficiency. Furthermore, an adaptive control model and achievement refinements of a micro-grid using Adaptive Neuro Fuzzy Inference System (ANFIS) controller has been utilized to regulate the load voltage and frequency. This suggested microgrid system is achieved so that the wind generation unit supplies the loads, while any additional energy needed by the loads will be offset by the fuel cell generator unit. Thus, the main objective of this work is to apply an adaptive control method for improving the proposed electrical micro grid performance. In addition, the performance of the considered system is compared with the proposed ANFIS control when applying the traditional fuzzy control. The outcomes also demonstrated a better reaction and durability to the chosen control model. The MATLAB/SIMULINK programming software tools have been used for carrying out case studies towards the evaluation and validation of the methodology developed in this work with applications. The proposed solution achieved improvement in transient performance. However, the settling time is decreased to 21% in the case of using the suggested ANFIS controller comparing with conventional fuzzy control.

1. Introduction

Electric power generation employing non-classical sources are gaining significant consideration all through the world because of the depleting of petroleum products, to ensure sustainability of the environment. Wind energy is among one of the important sources of energy typically utilized as an alternative to fossil fuel [1,2].

In general, some types of generating units are described by networks of small damping and a lack of control in the reactive power, and this may be the cause of some unexpected deviations of voltage and frequency as they are often located outside the grain boundaries [3]. But it may ensure a good storage system in an isolated generation system that serves to supply the loads with the desired power [4]. So, when wind energy conversion (WEC) systems are used to obtain renewable energy, many of them may use different generators to configure and construct these systems [5–8]. Kumar and Joshi [9] have increased the maximum power harvest, minimal harmonics at the output and the idea exhibits improved dynamic performance in the face of unpredictable wind velocity changes as well as changes in the load. The study of induction motors (IM) drive supplied by a hybrid wind/battery storage was studied by Abdalla and Abdullah [10] in which the regulator used was optimized using the Mine Blast Algorithm. That investigation utilized IM field-oriented velocity control as a separate

* Corresponding author.
E-mail address: aashiref@graduate.utm.my (S.A. Abdalla).

Peer review under responsibility of Ain Shams University.

Production and hosting by Elsevier

https://doi.org/10.1016/j.asej.2021.101655
2090-4479/

dynamic load and battery as a storage energy element. Due to the use of the independent wind power system, the quality and fineness of the energy balance was ensured by having battery units. The ideal pattern is constructed to be integrated with an uncontrolled rectifier, an induction motor, a permanent magnetic synchronous generator (PMSG), a lead–acid battery (LAB) as well as a buck converter.

Generally, wind turbines need appropriate control of their velocities in order to match with the wind speed and to obtain maximum electrical power from them. Many theoretical and practical studies have been done to model the components of the wind turbine system in order to control its various speeds, or to maximize the amount of energy produced. Therefore, Murugesan et al. [11] considered the experimental and theoretical effectiveness of a semi-empirical fuel cell type for examining the water dynamics on the electrical attitude of a 5 kW Ballard stack framework utilizing Nafion 117 polymer membrane for the influence of water dynamics of its electrical action. Vuppala et al. [12] discussed the optimization of membrane electrode assembly of polymer electrolyte membrane fuel cell using the response surface technique and a confirmed two-phase PEMFC numerical example is performed. Tijani et al. [13] presented the effect of different temperature and pressure on the running of voltage of polymer electrolyte membrane electrolyzer. Chien et al. [14] introduced a type of wind farm system that depicted the ability to trace a set point under discontinuous wind situations. The features of this pattern were also demonstrated in the depiction of the setpoint process under automatic generation control through emulation. Wilk and Węcel [15] presented an analysis of the proton exchange membrane fuel cells by a transient process. Lamus et al. [16] described a single proton exchange membrane fuel cell as a devoted energy source for high inductance superconducting coils. Martín et al. [17] investigated the performance modeling of the proton exchange membrane fuel cell for both dynamic and steady state experimental effectiveness. Razzak et al. [18] studied a DC-DC converter-based proton exchange membrane fuel cell pattern simulation due to the relations electrical and thermal styles.

Smart control technologies like fuzzy logic, artificial neural networks, fuzzy inference system and neuro-fuzzy have been found to be an effective alternative to classical technologies. An effective and intelligent control using adaptive neuro-fuzzy inference system (ANFIS) has been suggested by several authors in this field. So, Fathy and Kassem [19] discussed optimal load frequency control schemed by Adaptive Neuro Fuzzy Inference System (ANFIS) applied through Antlion optimizer for multi-interconnected framework including photovoltaic and wind turbine. Eshetu et al. [20] applied Adaptive Neuro Fuzzy Inference System ANFIS on the basis of load frequency control in an isolated micro grid. ANFIS is also compared with classical proportional-integral-derivative (PID) controller and fuzzy controller proposal procedures. Hussain et al. [21] demonstrated an application of ANFIS hybrid patterns to predict long-term wind energy intensity with extrapolation potential. Kanagasakthivel et al. [22] displayed a solar energy and hybrid wind model with ANFIS Considering the maximum power point tracking controller.

Recently, a lot of research has used the control method. However, there are fundamental differences in the structure of the system and the operating characteristics of its units. Among these researches, we mention the following. García et al. [23] considered and estimated an adaptive neural-fuzzy inference system (ANFIS) provided that energy management system (EMS) of a grid-connected hybrid system, This system is composed of renewable energy sources (WT and PV panels), hydrogen (FC, electrolyzer, and hydrogen tank), and battery. ANFIS- on the basis of control for the three-phase inverter, which connects the HRES to the grid. Neelima et al. [24] introduced a control system which coordinated the operation of multiple distributed generator (DG) transformers in a small network for both on-grid and tidal operations. The suggested controller for the DG inverters is considered as a newly advanced ANFIS controlled. Indeed, this paper considers close to our work with some fundamental differences, for example: in our work, we have standalone supply IM and static load only, DC link is considered as DC-AC converter, while the storage unit is taken as fuel cells. Amin et al. [25] developed ANFIS according to the control system for standalone operation mode of DFIG-WECS. The suggested controller focuses on organizing the frequency and the terminal voltage to a fixed value. The simulation controller durability is proven under variable conditions. Falehi and Rafiee [26] illustrated that some prospective disturbances impact the power framework with a view to check and confirm the implementation of the proposed DVR. Jurado et al. [27] displayed the design of a new fuzzy logic regulator for a three-phase inverter applying the procedure of inverter flux vector control style. In addition, an Adaptive-Network according to Fuzzy Inference System (ANFIS) is used. Mohanty et al. [28] describing a non-linear controller in the context of ANFIS with regard to unified power flow control (UPFC) slip mode control for modeling of the hybrid isolated power system. So, the UPFC sliding mode control module considers the parameter uncertainties and cancel out the nonlinearity. Reddy and Sudhakar [29] considered an adaptive neural-fuzzy inference system (ANFIS) on the basis of MPPT controller for the proton exchange membrane fuel cell (PEMFC) system utilized in electric vehicle applications.

While, Nazar et al. [30] investigated an ANFIS according to advanced maximum power point tracking (MPPT) control of a wind-solar standalone hybrid power generation model. Due to the instantaneous variable nature of the sun's temperature and insolation level, it is essential to specify the optimal voltage that will ensure maximum power output. Subha and Nagalakshmi [31] discussed the combination and control automation of renewable energy sources such as PV system, solid oxide fuel cell (SOFC) with nickel-metal-hydride (Ni-MH) battery jointly with a changing load existing in an SG. Bogaraj and Kanakaraj [32] displayed an energy management mechanism for Hybrid Renewable Energy System (HRES) linked with AC load employing Adaptive Neuro Fuzzy Interference System (ANFIS). So, Photovoltaic (PV) system, Wind Generating System (WGS), Fuel Cell (FC), Ultra Capacitor (UC) and the battery are treated as the energy sources.

Generally, These new ideas that may be added to our proposed system PV to be our next area of research with thinking about some other suggestions that help to improve the results and maximize the utilization of the outputs while reducing the energy loss factors required to be obtained. For further clarification and explanation of the methods used, the type of control used, and the basics of the topics presented in this work, useful references can be viewed for this purpose (see Refs. [33–39]).

Furthermore, recently Priyadarshi and his co-authors [40,41], based on Maximum Power Point Trackers (MPPT) devices, many control systems have used in order to obtain optimal photovoltaic power. For example, they have utilized an intelligent fuzzy particle swarm optimization (FPSO), an adaptive neuro-fuzzy inference system-particle swarm optimization (ANFIS-PSO), grid-integrated system with Lyapunov function and a Particle Swarm Optimization (PSO) augmented Internet of Things (IOT).

This paper presents a control simulation of an isolated hybrid electrical system powered by a wind turbine coupled to a fuel cell-based storage system. In more details, a microgrid including wind power and fuel cell as generation units which supply both static and dynamic loads are presented. Thus, The essential contribution of this paper are: (i) The application an ANFIS control algorithm for many reasons such as: Improving the proposed electrical micro grid performance of stand-alone hybrid renewable energy systems, stabilizing the AC load voltage to have constant amplitude and frequency, achieve refinement in transient performance as well as the mathematical problems separately. (ii) This intelligent control system is useful to determine the power that must be generated by storing in the energy storage system of the fuel cell considering the power demanded by the load, the available power and the hydrogen tank level. (iii) The ANFIS control system is also applied to the inverter due to the precise control of the power delivery to the system by means of charge/discharge power as control parameters. (iv) Finally, due to the validation of the proposed ANFIS control, conventional fuzzy control is applied.

So, this paper will be organized as follows: Section 2 presents the configuration for the suggested model. Section 3 gives mathematical modeling and the main equations necessary for the other subsections of the research. In Section 4 the structure of ANFIS controller is explained with a description of the necessary layers, a membership function as well as control operations with detailed diagram. Simulation results and graphical numerical calculations are provided in Section 5 while, the conclusions are presented in Section 6.

2. Design configuration of the proposed hybrid system

The suggested scheme consists of a hybrid wind/FC power generation unit supplying static and dynamic loads, as presented in Fig. 1. The proposed system mainly consists of wind turbine drive PMSG, fuel cell generation unit, uncontrolled rectifier, DC-AC inverter, static and dynamic loads. The static load is proposed to be a general inductive resistive load has a specific resistance. The dynamic load on the other hand, is an induction motor whose speed is controlled. These loads are provided for the suggested hybrid wind/FC generation unit by means of an inverter. This inverter is regulated by a method to feed the suggested dynamic and/or static loads through a controlled AC voltage. The input to the inverter is the DC bus voltage which is linked to the fuel cell output as well as the PMSG. The electrolizer of water is used as well as it is supplied with the amount of energy produced in obtaining high wind energy to generate hydrogen gas, which can be saved for use as fuel for the fuel cell generator [10].

It is known that the energy obtained from the wind varies due to the change of wind velocity. Consequently, the AC voltage generated by the PMSG changes at both frequency and amplitude. Subsequently, in this case the fuel cell generator unit is utilized to provide power to the necessary loads in the event that the wind generator unit energy is low. Hence, it acts as a server to compensate for any shortage of wind energy generated and/or other additional energy that the loads may need.

3. Mathematical modelling and principal equations

The wind energy conversion system may be split into interlinked sub-models as illustrated in Fig. 1.

3.1. Mathematical modelling of wind turbines

Wind energy is considered as the one of the most important renewable energy sources for its widespread use as well as being highly desirable in the clean energy industry. The relationship between turbine power and wind speed is given by the following formula [14]:

$$P_m = \frac{1}{2}\rho A C_p(\beta, \lambda) V_\omega^3 \tag{1}$$

The tip speed ratio is of great importance for blade design by various formats which may be written as:

$$\lambda = \frac{\omega_t r}{V_\omega} \tag{2}$$

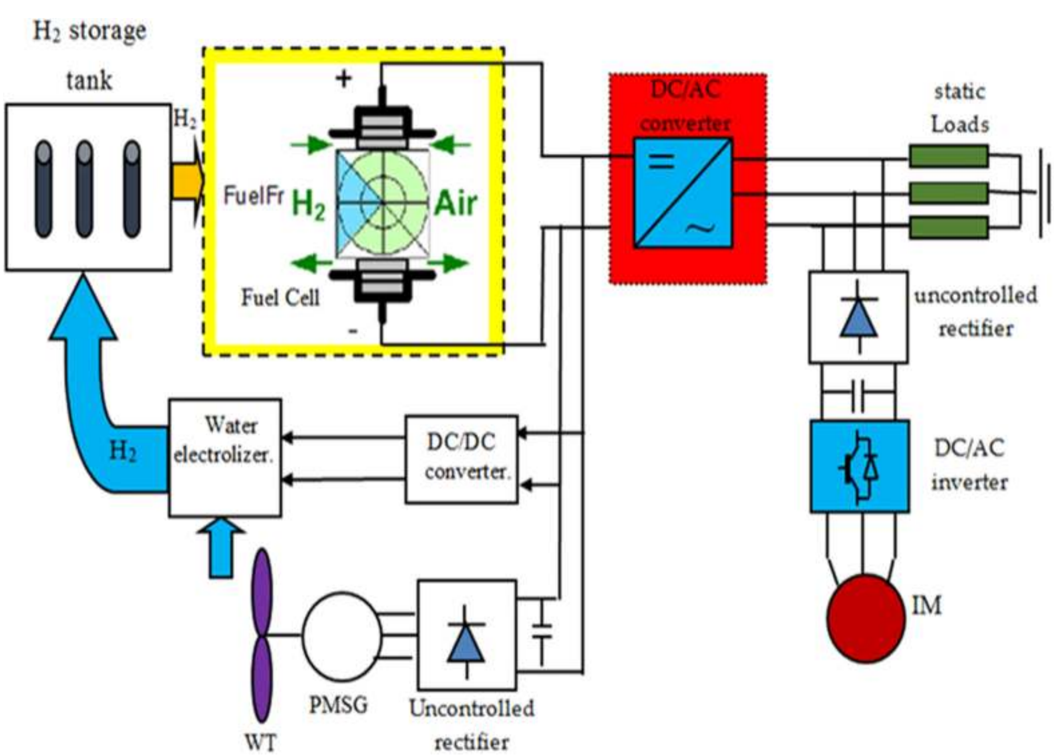

Fig. 1. Schematic diagram of a grid hybrid wind-fuel cell generation unit supplying static and dynamic loads.

The power coefficient C_p is extremely significant as it is responsible for the efficiency of the turbines that convert wind energy into electricity. Note that C_p has a non-linear relationship with both λ and β and one may obtains in the following form which can be validated practically [13,15]:

$$C_p(\beta,\mu) = c_1\left(\frac{c_2}{\mu} - c_3\beta - c_4\beta^{c_5} - c_6\right)\exp\left(\frac{-c_7}{\mu}\right). \tag{3}$$

where

$$\frac{1}{\mu} = \frac{1}{\lambda + c_8\beta} - \frac{0.035}{\beta^3+1}. \tag{4}$$

where $c_i, i = 1, 2 \cdots, 8$ are the constant parameters of turbine blade which are given in Table 8 in Appendix 1. Also, the wind turbine torque T_m is expressed as:

$$T_m = \frac{1}{2}\rho ARC_T V_\omega^2. \tag{5}$$

Therefore, the wind turbine torque coefficient C_T is considered as $C_T = \frac{C_p}{\lambda}$. Fig. 2a exhibits the variation of C_p versus λ for different pitch angle β.

Also, it is obvious that when β gradually grows, the value of C_p minimizes significantly, for example, at $\beta = 5^o$ and $\lambda = 8.9$, the maximum value of C_p that is $C_{p_{max}} = 0.286$. So, the special value λ_{opt} produces the optimum efficiency point since the maximum energy is held from wind through wind turbines. The values for the variables $C_{p_{max}}$, β and λ_{opt} can be shown in Table 1. Generally, control of blade pitch is an important and effective component in facilitating reduced load during conserving energy capture production. Therefore, the information that may be abstracted from Figs. 2a–2c may be used to become an essential guide to help in the pitch angle control (PAC). It is also an indispensable mechanism in the case of the variable velocity of the wind turbine to provide energy schemes or limit energy production in the case of high-velocity wind [34]. Moreover, it is often preferred to calculate the turbine rotor velocity (ω) rather than the wind speed V_ω to obtain maximum power point tracking technique (MPPT). Figs. 2b and 2c exhibit wind turbine energy and turbine torque energy against the rotor speed for different wind velocities. Therefore, from Figs. 2b and 2c, it is possible to know MPPT values that may be obtained at different rotor speeds. For instance, see the Tables 2 and 3 [19]. Note that, the graph of the MPPT curves appears in black in Figs. 2a–2c.

3.2. PMSG mathematical formulation

The mathematical formulation of the voltages and currents concerning the permanent magnet synchronous generators (PMSG)

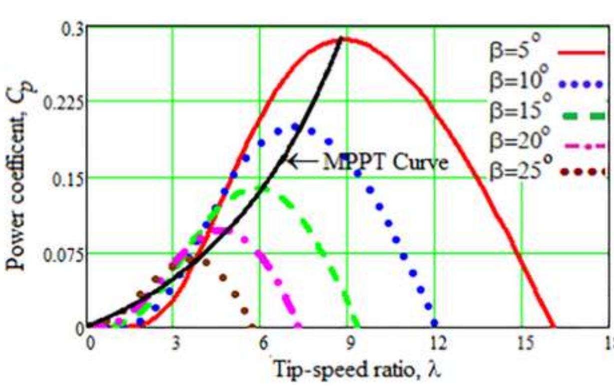

Fig. 2a. C_p against λ curves for different pitch angle.β.

Table 1
The relations between $C_{p_{max}}$, β and λ_{opt}.

Pitch angle β	λ_{opt}	$C_{p_{max}}$
$\beta = 5^o$	8.9	0.286
$\beta = 10^o$	7.3	0.199
$\beta = 15^o$	5.7	0.139
$\beta = 20^o$	4.5	0.096

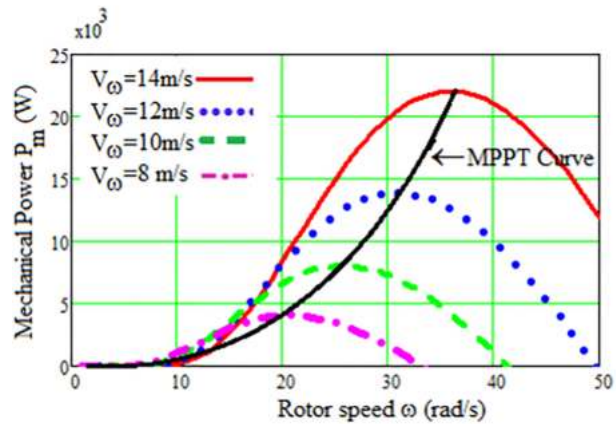

Fig. 2b. P_m against ω for different wind speeds..

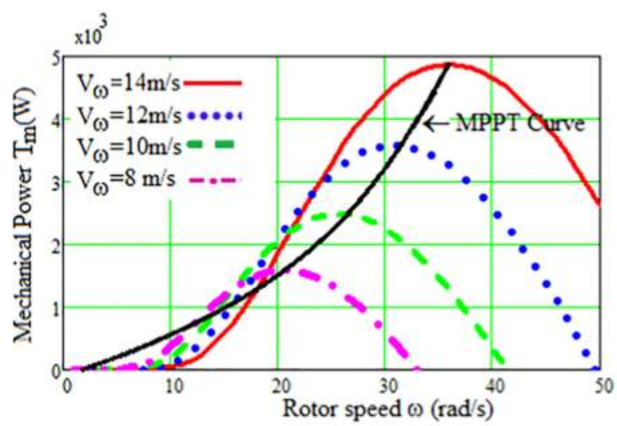

Fig. 2c. T_m against ω for different wind speeds..

Table 2
The relations between $P_{m_{max}}$, V_ω and ω_{opt}.

V_ω (m/s)	ω_{opt}	$P_{m_{max}}(10^3)$
8	21	4.099
10	26	8.015
12	31	13.856
14	35	21.957

Table 3
The relations between $T_{m_{max}}$, V_ω and ω_{opt}.

V_ω(m/s)	ω_{opt}	$T_{m_{max}}(10^3)$
8	21	1.588
10	26	2.485
12	31	3.580
14	36	4.873

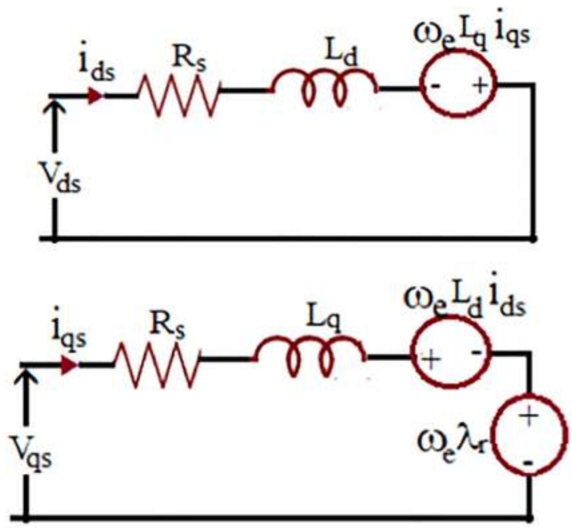

Fig. 3. Equivalent Circuit of PMSG.

may appear in the direct quadrature (d-q) order system, that may be written as a following tensor form, see Fig. 3 [22]:

$$V_{ds} = R_s i_{ds} - \omega_e L_q i_{qs} + L_d \frac{di_{ds}}{dt} \tag{6}$$

$$V_{qs} = R_s i_{qs} + \omega_e(\lambda_r - L_d i_{ds}) + L_q \frac{di_{qs}}{dt} \tag{7}$$

The fundamental dynamical angular velocity of the turbine described as follows [10]:

$$J\frac{d\omega_r}{dt} = T_m - T_e \tag{8}$$

where T_e is the electromagnetic torque and is expressed as follows:

$$T_e = \frac{3}{2}\frac{P}{2} i_q \lambda_m \tag{9}$$

Eqs. (6) and (7) give configuration about the circuit organizations which are suitable representation of the electrical equivalent of PMSG in the *d* axis and the basis of the *q* axis. The electrical circuit of the PMSG is displayed in Fig. 3. There exist three-phase windings and phase windings have a constant resistance, mutual inductor and self-variable position.

3.3. Uncontrolled rectifier pattern

Since the wind velocity depends on time, thus the velocity of the PMSG rotor changes**.** Hence, the AC output voltage of the PMSG oscillates in power and frequency. Therefore, an uncontrolled dual conductor rectifier is utilized to change the alternating output voltage PMSG to a variable DC voltage and current which may be expressed as [10]:

$$V_{DC(rect)} = \frac{3\sqrt{3}}{\pi} V_g = 1.654 V_g$$

$$I_{DC(rect)} = \frac{\pi}{2\sqrt{3}} I_{g(rms)} = 2.721 I_{g(rms)}$$

3.4. Mathematical formalization of PEM fuel cell

Next, the modeling of the physical–chemical reactions in the proton exchange membrane (PEM) fuel cell will be examined. The equations given in this section help to foretell the speed at which the reactants are transformed into electrical current as well as the amount of energy loss that manifests through the present electrochemical reaction. The fuel cell potential V_{fc} of a single cell at any instance may be presented as follows [15–17]:

$$V_{fc} = E - V_{act} - V_{ohm} - V_{con} \tag{10}$$

where the definition of the various parameters is given in Appendix A1.

Various factors cause the fuel cell voltage to reduce to make the voltage of the cell lower than its optimum power. Generally, it has been found that losses arise mainly from the following three classes of voltage drop: the concentration (V_{act}), ohmic (V_{ohm}), and activation (V_{con}) over voltages.

The thermodynamic potential E illustrates the reverse voltage. Theoretically, it is calculated considering the energy balance between the reactants and products. It may be written as [18,37]:

$$E = -\frac{G}{2F} - \frac{RT_k}{2F}\ln\left(\frac{P_{H_2O}}{P_{H_2}P_{O2}^{1/2}}\right) \tag{11}$$

The activation over voltage equation is given by the Tafel equation as:

$$V_{act} = \frac{RT}{\alpha_t F}\ln\left(\frac{i + i_{loss}}{i_o}\right) \tag{12}$$

The ohmic losses are obtained using Ohm's law as:

$$V_{ohm} = iR_i \tag{13}$$

Concentration over-voltage may be calculated using from:

$$V_{con} = \frac{RT}{nF}\ln\left(\frac{i_L}{i_L - i}\right) \tag{14}$$

The polarization graph, Fig. 4, is of immense significance for the study and development of fuel cell properties and efficiency.

It consists of three different regions, each of which corresponds to the influence and performance of a polarization type: In the first region, the activation polarization appears mainly in currents whose value is small and then decreases when the current density rises. In the second region, ohmic polarization is linearly decreased with current density growth. Finally, in the third region, concentration polarization occurs at high marginal currents.

It should be noted the following:

- V_{act} occurs due to the activation of the anode and cathode and due to the slow interactions, that occur within the cell. The catalyst contact area for reactions may be maximized to reduce this term.

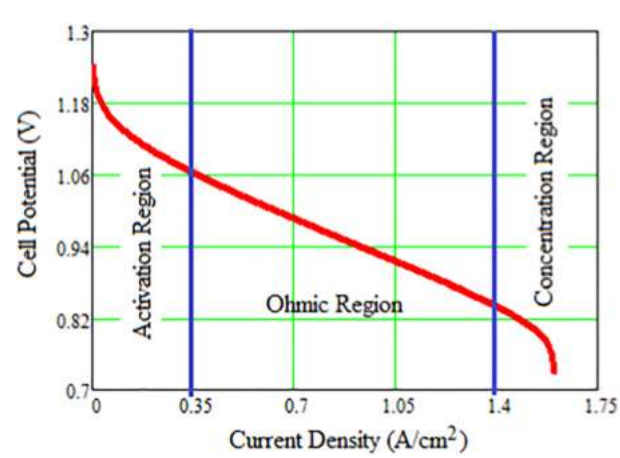

Fig. 4. PEM fuel cell polarization graph.

- V_{ohm} takes into account resistance while protons are connected through an electronic and, solid electrolyte along its pathway.
- V_{con} is responsible for the diminution of the voltage due to the low concentration of the reactive gases. Finally, resistive losses happen because of the flow of current that result in resistance of the perfect electrical circuit inclusive the connections and membrane.

3.4.1. Sensitiveness of some variables to the polarization curve

(i) Effect of Transfer Coefficient (α_t).

In Fig. 5a displays fuel cell achievement with "$\alpha_t = 0.5, 0.7, 0.9, 1.1$". In order to develop the completion and operation of the fuel cell with full efficiency and the design of other modern types, there is an urgent need to understand and determine the transfers of charges between the cathode and the anode into the fuel cell. Therefore, the charge transfer parameter α is an important factor for electrochemical reactions of the cathode and anode inside the fuel cell. It has a strong impact on the fuel cell achievement [13].

(ii) Exchange Current Density Impact.

From Fig. 5b, the significance of exchange current density i_o may be obviously visible and it is the critical parameter in contraction the activation overvoltage. It displays polarization diagram for four various values of i_o, i.e., $i_o = 3(10^{-3}, 10^{-4}, 10^{-5},\ 10^{-6})$. It is noted that a decrease in i_o, the current density reduces the cell voltage by a constant amount. Therefore, higher value of i_o, performs in better fuel cell achievement. So, from the laboratory point of view, it is possible to measure this extra voltage at each electrode, either by using reference electrodes inside a working fuel cell or by using half-cells (see Ref. [11,12]). Moreover, with an increase of i_o, especially in the cathode, the cell performance will be improved [35].

(iii) Internal Resistance Impact

Fig. 5c illustrates the effect of change in typical values for the internal resistance $R_i = (0.1, 0.15, 0.2, 0.25)$ on polarization curve. It is noted that the internal resistance impact is directly proportional with current density. The values above 0.2 $ohm.cm^2$ would refer unsuitable chosen of cell materials as well as deficient contact pressure [35].

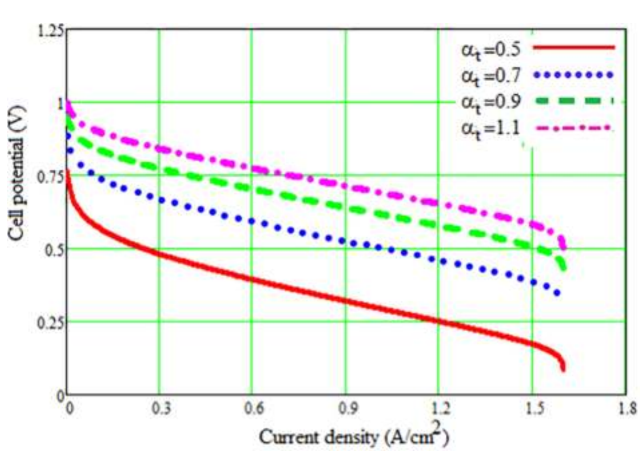

Fig. 5a. Influence of α on the behavior of a fuel cell.

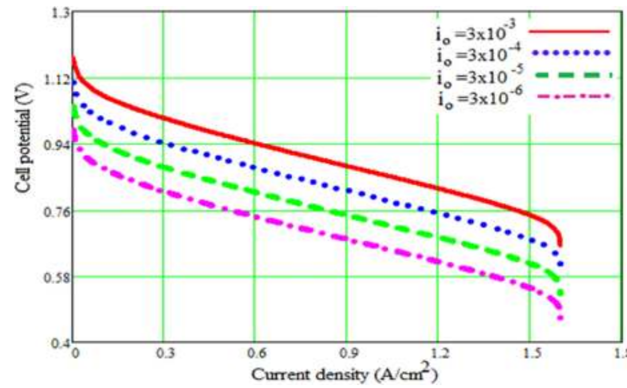

Fig. 5b. Exchange current density Impact polarization diagram.

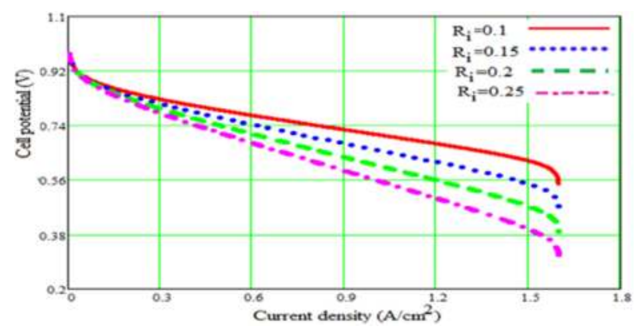

Fig. 5c. Internal resistance Impact on polarization diagram.

3.4.2. Fuel cell polarization scheme and its importance

One of the most significant characteristics of a fuel cell is the polarization curve. It helps in many ways to find out the optimal size of the fuel cell, its proper form and appropriate control methods for it, as well as diagnosing the appropriate method for its design. Moreover, knowledge of much other information about a fuel cell may only become available by rearranging potential current data.

3.5. Induction machine model

The rotor and stator voltage conditions of an induction machine in a synchronous casing are given in details in Ref. [10].

4. Adaptive neuro-fuzzy inference system (ANFIS)

Jang [38], was the first to introduce the expression of adaptive neuro-fuzzy inference system in 1993. ANFIS combines the learning ability of ANNs through the learning illustration of fuzzy logic to generate a robust and smart information model. The Fuzzy Inference System (FIS) is the centre of ANFIS through the algorithm for learning the neural network. The characteristics and usefulness of ANFIS which is consisting of neural network and fuzzy logic are:

- ANFIS considers the neural network's efficiency to categorize input and notice styles;
- It also develops a fuzzy expert style that is more straightforward to the employee and less likely to bring preservation errors from the neural network,
- Then, ANFIS can divide information into sets and modify these sets to get the best membership functions which collect information and derive the required outcomes through the lower time.

– Moreover, ANFIS has its origin from expertise relied on the rule's condition "IF-THEN".
– Therefore, it may be utilized to foretell the character of various undetermined models.

Fig. 6 illustrates a method for specifying the membership function (MF) parameters that better accept the fuzzy inference system accompanying tracking specific Input/Output information.

Layer 1:

This layer includes (MFs) of the input variables and passes the input data to the following layer. Every node in this layer is adaptable as a function like $B = \mu_A(x)$ to create MFs. So,

Layer 2:

Here will be the weights of MFs. The input data of this layer comes from the first layer. The result of this layer is the product of all the received signals and is given as:

$$w_i = \mu(x)_i.\mu(x)_{i+1}, \text{for} i = 1, 2 \quad (15)$$

The output of every node denotes the strength of the base's weight.

Layer 3:

In this layer, each node meets the prerequisites of the fuzzy rules, that calculates the activation level for each base and the normal activation force. This is a static layer as well, and each node calculates the ratio of the i^{th} principle of the firing strength to the total of the i^{th} powers of all the bases as:

$$w_i^* = \frac{w_i}{w_1 + w_2}, \text{for} i = 1, 2 \quad (16)$$

The outcomes of this layer are labelled as normal weights.

Layer 4:

This layer generates defuzzied outputs in the form of Takagi and Sugeno. The defuzzied estimation is being produced for each rule fired using the form:

$$S_i^4 = w_i^* f = w_i^*(p_i x + t_i) \quad (17)$$

where, the set of variables is given as $\{p_i, t\}$.

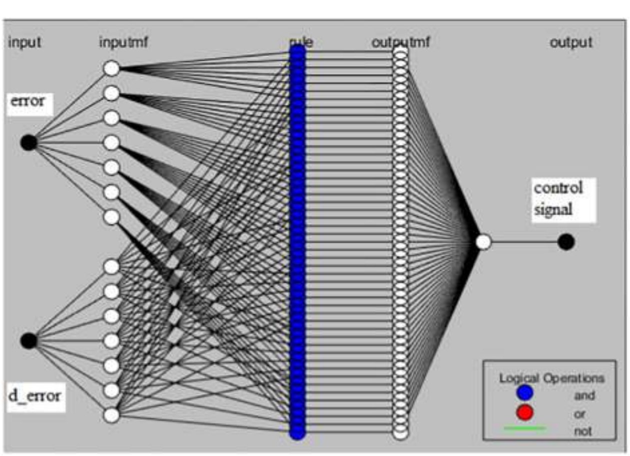

Fig. 6. The proposed ANFIS controller internal structure.

Layer 5:

Thus, the output layer that summarizes the inputs and outputs is from the previous layer. Therefore, the single node is a constant node, and the whole next signal is summarized to get the total result as:

$$S_i^4 = \sum_i w_i^* f = \frac{\sum_i w_i^* f}{\sum_i w_i^*} \quad (18)$$

ANFIS structure is mainly consists of five of the functional blocks (database, rule base, decision making unit, fuzzyfication interface, defuzzyfication interface) [24]. In this paper, The proposed designed ANFIS includes two inputs and one output where the first input is the error signl. The second is the derivative error signal, while the output of the ANFIS is the control signal which needed to track the desired load voltage.

Hybrid learning technique which combines both of the gradient descent and the least square with 300 epochs and 2365 training samples is applied to train the proposed ANFIS controller. Fig. 6, shows the internal structure of the proposed ANFIS controller.

5. Simulation results

Due to the ANFIS control technique is applied to adjust the DC-AC converter output voltage to its desired value as shown in Fig. 7. Therefore, the outcomes of digital simulation results to verify the efficiency of the hybrid generation technique studied through the change of wind speed and the variation in load parameters are obtained. The system mathematical model shown in Section 3, is used to implement the MATLAB-SIMULINK program and design the ANFIS needed control. The suggested composition of the micro-grid fuel cells/wind through the determined control procedure is represented in Fig. 8. This system has been simulated and tested using the MATLAB/SIMULINK programming software tools to accommodate multiple operating methods for wind velocity and load parameter changes. In this study, four different operating conditions are considered as:

Firstly, it is considered to vary the following:- (1) wind speed, (2) static load parameters and (3) IM rotor velocity as a disturbance. The simulation results of this case are illustrated in Fig. 9 in the context of various values of wind velocity, SG rotor velocity, the pressure of fuel cell for hydrogen and oxygen, SG stator current, produced energy from wind and fuel cell and load required energy, actual and reference load voltage, IM stator current, static load current, IM actual and required rotor velocity and IM torque.

Secondly, the results of this case are obtained as displayed in Fig. 10. In this case, it is investigated the enhancement of the mentioned model through the offered control technique on the basis of a step alteration of wind velocity, the step change in induction motor rotor speed.

Thirdly, in this case, the rotor speed of the induction motor is set constant, while the wind speed and the static load are varied.

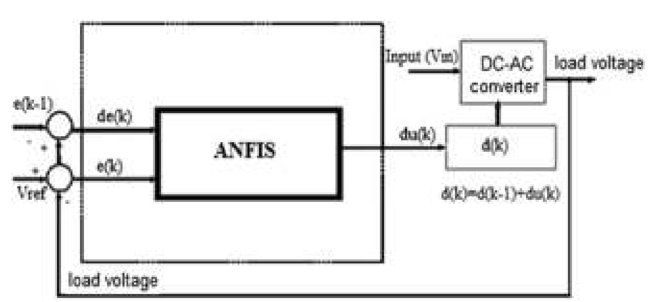

Fig. 7. ANFIS for Hybrid Wind/FC Energy System.

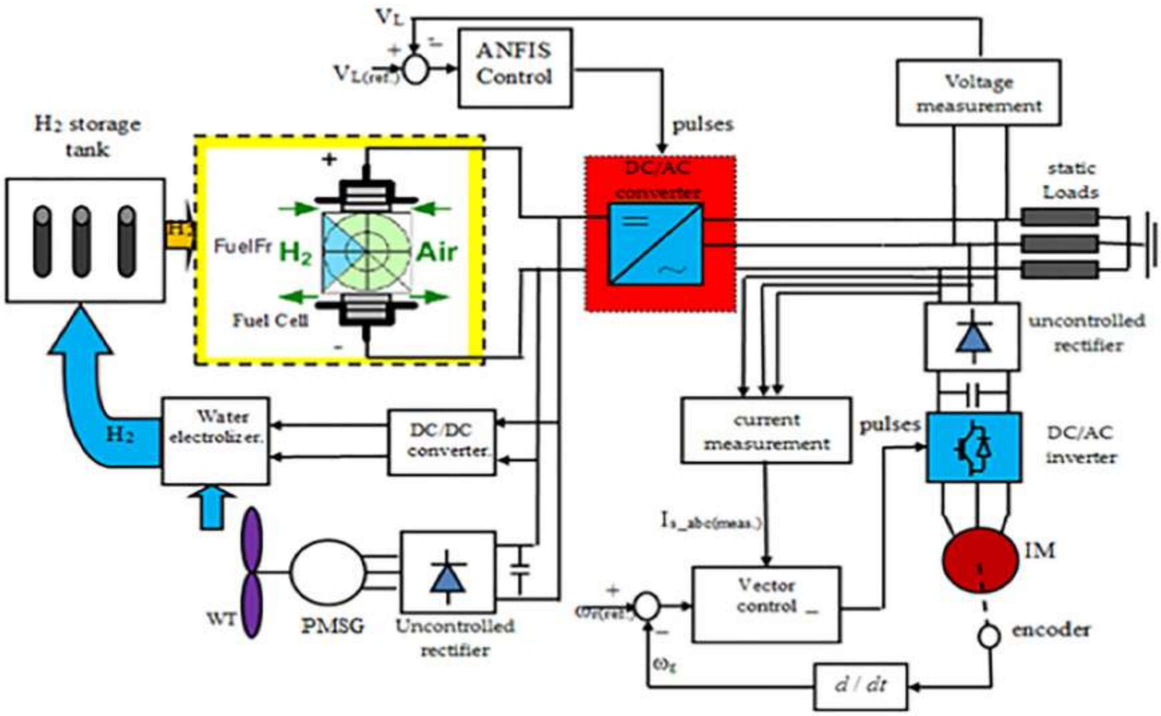

Fig. 8. The suggested microgrid power model and its controllers.

So, the results are considered according to a constant dynamic load as shown in Fig. 11.

Fourthly, the last case, only the wind speed is set constant, while the IM rotor speed and the static load are varied as shown in Fig. 12.

It is clear from the Figs. 9–12 the distinctions of the studied system by the change of various parameters for step modification in both wind velocity and static load impedance as well as changes of induction motor rotor speed considering that suggested controller. It should be noted that the data used in the numerical simulations are given in Appendix Table 9.

According to the obtained results, which were presented graphically as well as summarized in Tables 4–7, the following observations can be explained.

* Fig. 9A shows the wind speed (WS) as a function of time t. It is noticeable that the (WS) changes according to the change of time in the following three periods: t = (0–1.5), (1.5–4.5) and (4.5–6) and the values of WS in these periods are 14, 11, 13 m/s, respectively.

* Fig. 9B displays the SG rotor speed (RS) variations with time (t) due to variations of wind speed (WS). It is noted that the (RS) values become (370, 320, 358) rpm in the same devious three periods: t = (0–1.5), (1,5–4.5) and (4.5–6), respectively.

* Fig. 9C presents the SG torque versus variations with t due to variations of WS. It is observed that the torque values become (−13, −4.3, −9) Nm in the same three periods that were mentioned previously.

* Fig. 9D exhibits the SG stator current as variations with t due to variations of WS. The current values differ between two values as follows: (−15 to 15)A, (−8 to 8) A and (−11.6 to 11.6) A, in the same three aforementioned periods, respectively.

* Fig. 9E considers the SG stator voltage against t. It is found that at any time t the voltage is changed between (−370 to 370) V.

* Fig. 9F presents the P-H2 and P-O2 versus t. The values of P-H2 and P-O2 are the same (0.04 to 0.05) Pa in the first period of time (0–1.5) s. But they differ slightly as shown in Table 1.

* Fig. 9G describes actual and reference load voltage as a function of t. The load voltage takes the values (0.8, 0.9, 0.85) V in the following three periods: t = (0–1.5), (1.,5–4) and (4–6), respectively.

* Fig. 9H illustrates static load current against t. It is remarked that at the beginning the static amplitude load current (SALC) has the value 4A. Then, when t = 1.5 s, the (SALC) increases to become 4.8 A due to the growing of the frequency load voltage as shown in Figures 9G and 9H. After that, at t = 2 s, the SALC is increasing to 9.0A because of the diminishing of the load impedance. While, at t = 4 s the SALC reduces again to become 8.5A owing to the decreasing of the reference voltage. Also, at t = 4.5 s, the SALC declines to 4.0A due to the rising of load impedance.

* Fig. 9I investigates static load voltage (ALV) with the change of t. It is seen easily that in the first period t = (0–1.5) s, the amplitude of (ALV) becomes 175 V. While, in the interval (1.5–6) s, the amplitude of (ALV) increases to reach to 182 V.

* Fig. 9H and I show that the load voltage frequency is adjusted at its reference value 60 Hz. The same can be illustrated in the other cases.

* Fig. 9M explains IM stator voltage against of time. It is noticed that IM stator voltage has the values between (−370 to 370) V in the interval t = (0–6) s.

* Fig. 9N discuss IM stator current versus t. It is obvious that at t = 2.5 s, its frequency decreased from 11 to 8 Hz owing to the variation in rotor speed as shown in Fig. 9M and O.

* Fig. 9O examines IM rotor speed depending on time. It is noticed that through the first period t = (0–2.5) s, the IM rotor speed becomes 37 rad/s. While, in the next period t = (2.5–6) s, the IM rotor speed reduced to 25 rad/s.

A similar detailed explanation is quite clear using the Figs. 10–12 as well as the Tables 5–7 that can be performed in the other cases. However, we generally conclude the following general observations:

The diminution of the wind velocity brings to detraction in the generator rotor velocity. This happens when using PMSG as

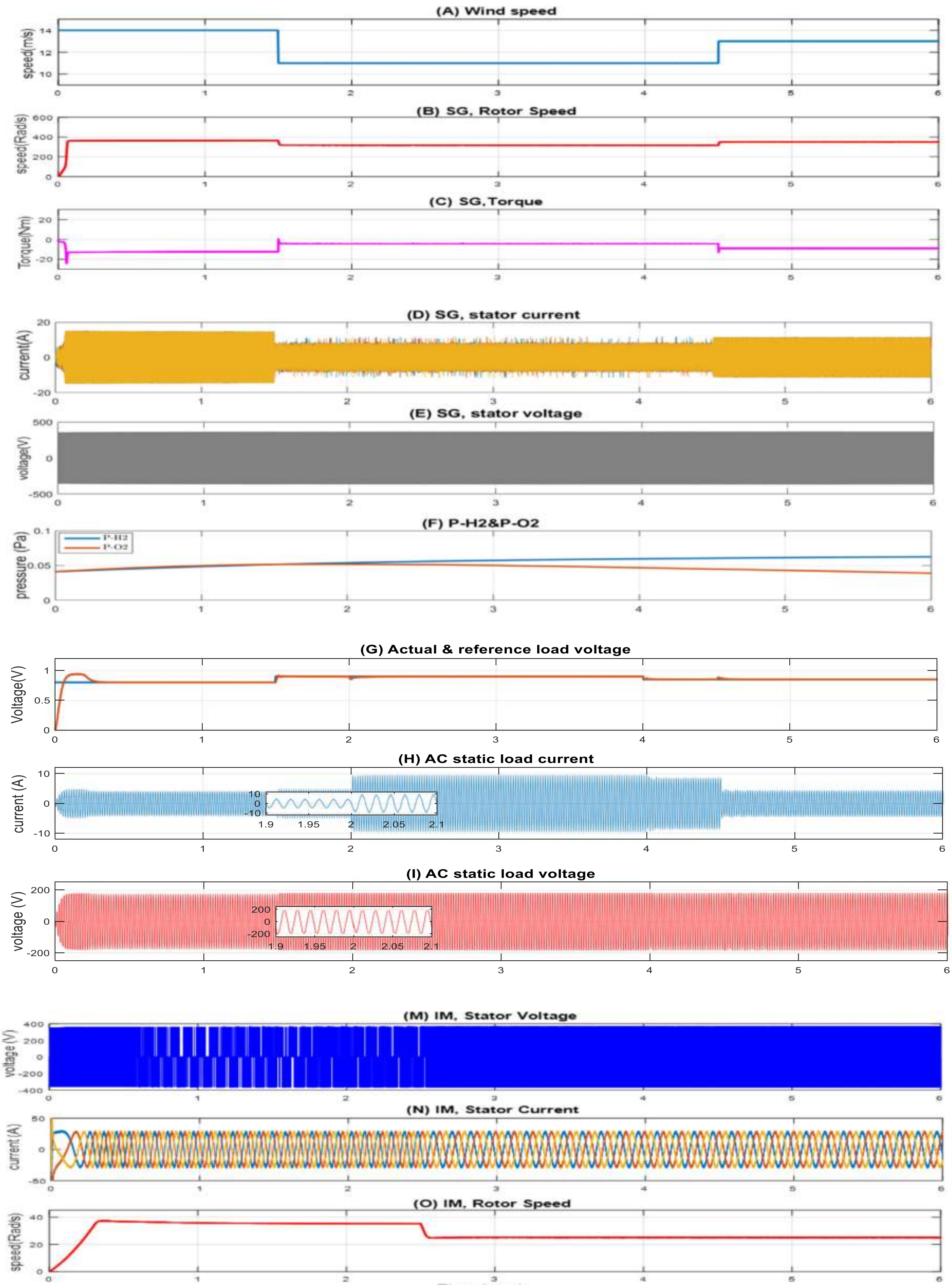

Fig. 9. Time response of the proposed system based on ANFIS control in case of wind speed, static load parameters and IM rotor velocity variations.

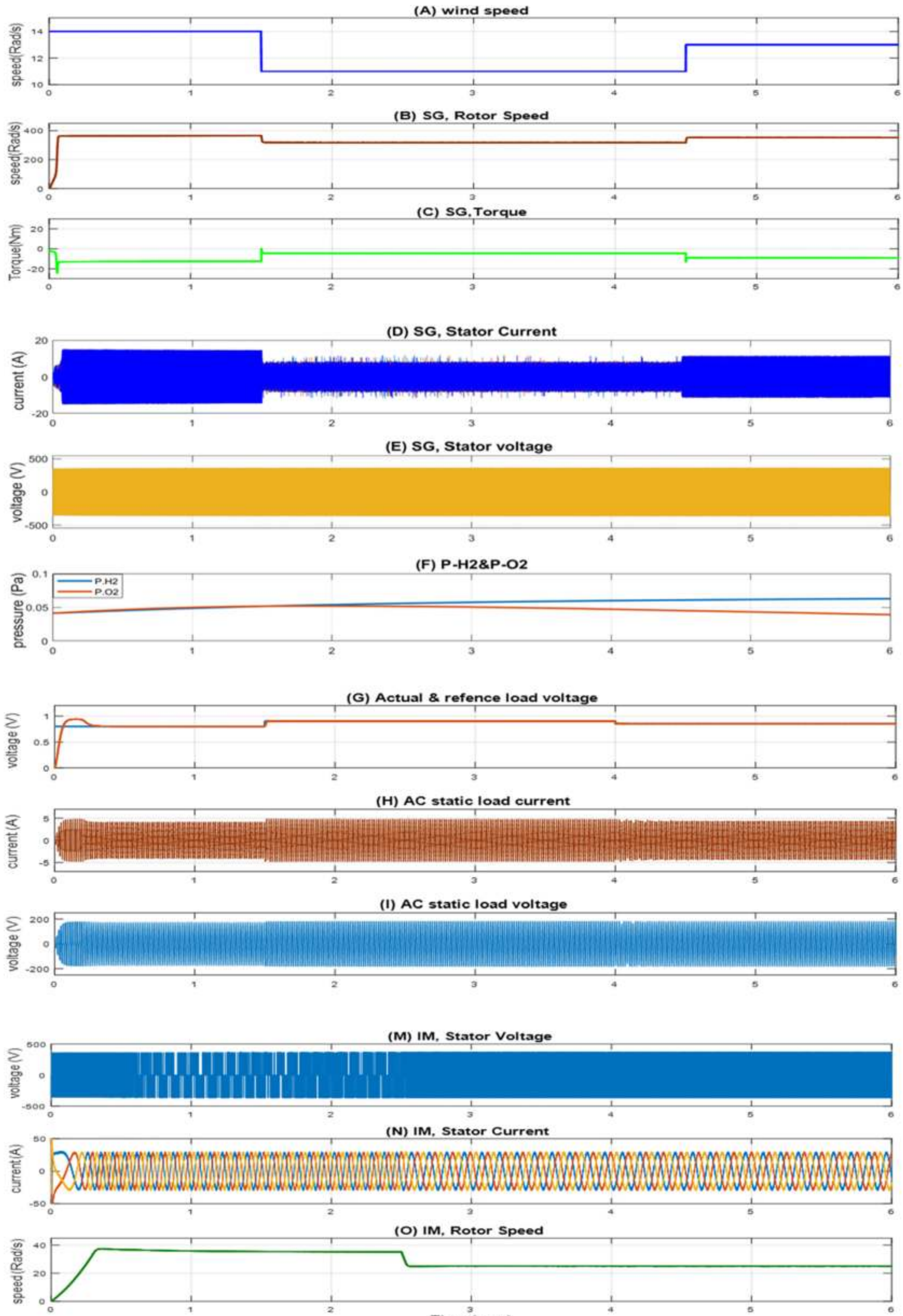

Fig. 10. Time response of the proposed system based on ANFIS control in case of step variation in wind velocity and step change in induction motor rotor speed.

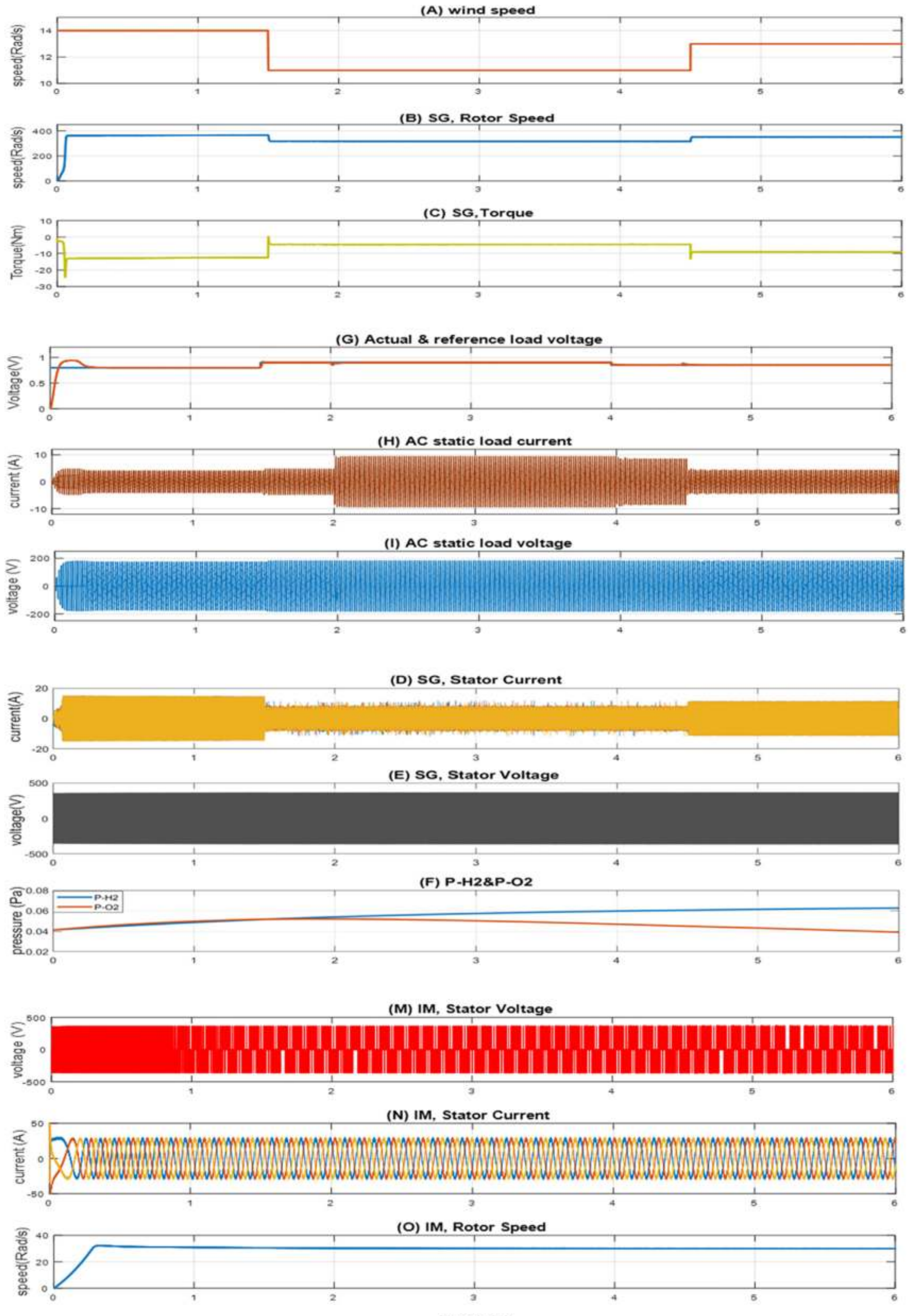

Fig. 11. Time response of the proposed system based on ANFIS control in case of step variation in wind speed and the static load.

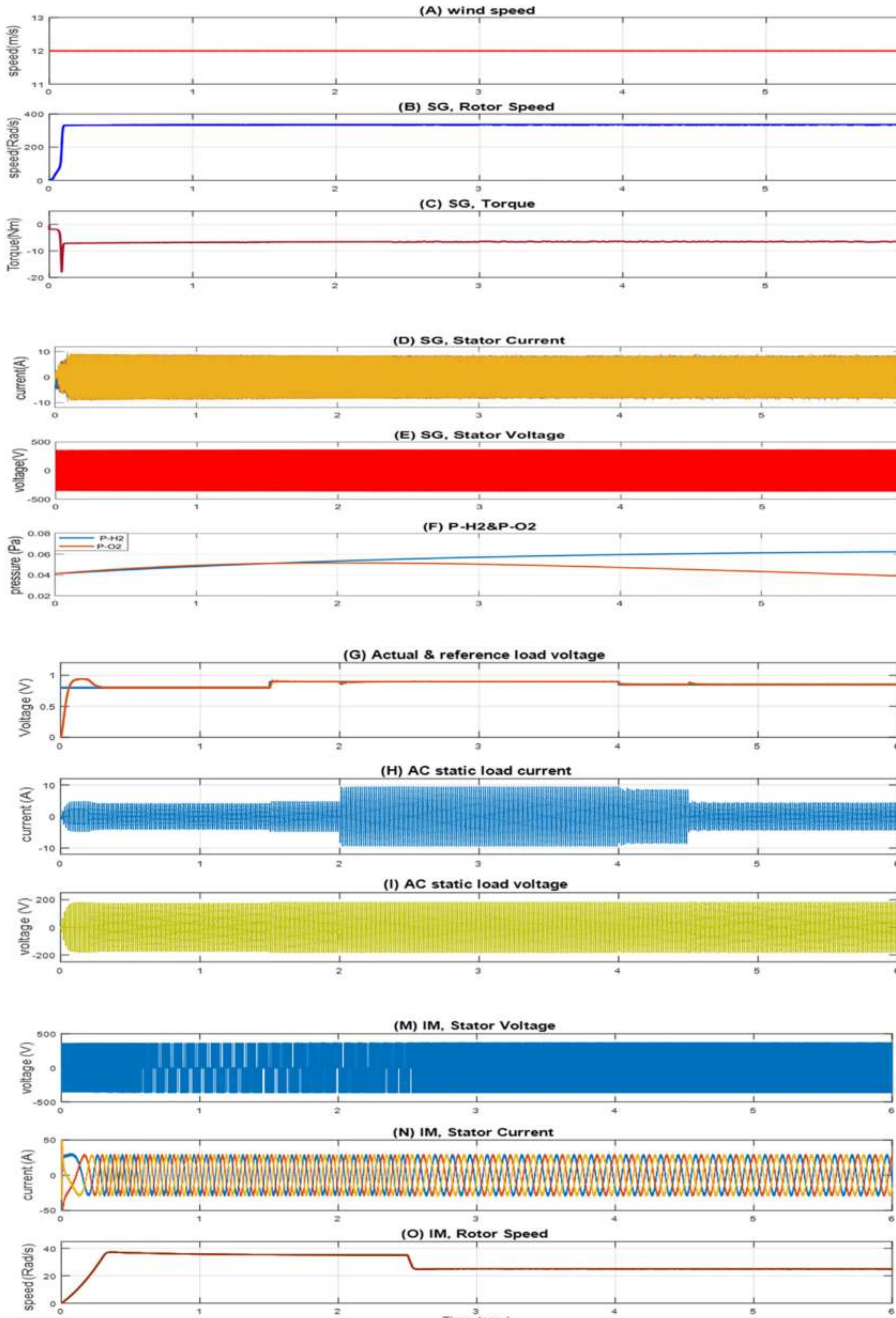

Fig. 12. Time response of the proposed system based on ANFIS control in case of step variation in IM rotor speed and the static load.

Table 4
Reactivity effect of independent wind/fuel cell supply the production constituent IM and static load through the considered control for step changes in wind velocity during modifies in IM rotor speed and static load.

Figure No.	The different Variables on y-axis	Time Variable on time-axis		
		(0–1.5) s	(1.5–4.5) s	(4.5–6) s
Fig. 10A	Wind speed (m/s)	14 m/s	11 m/s	13 m/s
Fig. 10B	SG rotor speed (rad/s)	370 rpm	320 rpm	358 rpm
Fig. 10C	SG torque (Nm)	−13 Nm	−4.3 Nm	−9 Nm
Fig. 10D	SG stator current (A)	(−15 to 15) A	(−8 to 8) A	(−11.6 to 11.6) A
Fig. 10E	SG stator voltage (V)	(−370 to 370) V		
Fig. 10F	P-H2 (Pa) P-O2 (Pa)	(0.04 to 0.05) Pa (0.04 to 0.05) Pa	(0.05 to 0.06) Pa (0.05 to 0.045) Pa	(0.06 to 0.062) Pa (0.045 to 0.039) Pa
Fig. 10G	Actual & Reference load voltage (p.u)	(0.8) p.u	0.9p.u At (1.5 to 4) s	0.85p.u At (4 to 6) s
Fig. 10H	AC static load current (A)	At (0 to 1.5) s (−4. to 4.) A At (1.5 t0 2) s (−4.8 to 4.8) A	At (2 to 4) s (−9 to 9) A	At (4 to 4.5) s (−8.5 to 8.5) A At (4.5 to 6) s (−4 to 4) A
Fig. 10I	AC static load voltage (V)	(−175 to 175)V	(−182 to 182)V	
Fig. 10M	IM stator voltage (V)	(−370 t0 370) V		
Fig. 10N	Frequency of IM stator current (Hz)	At (0 to 2.5) s 11 Hz	At (2.5 to 6) s 8 Hz	
Fig. 10O	IM rotor speed (rad/s)	At (0 to 2.5) s 37 rad/s	At (2.5 to 6) s 24.6 rad/s	

Table 5
Reactivity effect of independent wind/fuel cell supply the production constituent IM and static load through the considered control for step changes in wind velocity and IM rotor speed.

Figure No.	The different Variables on y-axis	Time Variable on time-axis		
		(0–1.5) s	(1.5–4.5) s	(4.5–6) s
Fig. 11A	Wind speed (m/s)	14 m/s	11 m/s	13 m/s
Fig. 11B	SG rotor speed (rad/s)	370 rpm	320 rpm	358 rpm
Fig. 11C	SG torque (Nm)	−13 Nm	−4.3 Nm	−9 Nm
Fig. 11D	SG stator current (A)	(−15 to 15) A	(−8 to 8) A	(−11.6 to 11.6) A
Fig. 11E	SG stator voltage (V)	(−370 to 370) V		
Fig. 11F	P-H2 (Pa) P-O2 (Pa)	(0.04 to 0.05) Pa (0.04 to 0.05) Pa	(0.05 to 0.06) Pa (0.05 to 0.045) Pa	(0.06 to 0.062) Pa (0.045 to 0.039) Pa
Fig. 11G	Actual & Reference load voltage (p.u)	(0.8) p.u	0.9p.u At (1.5 to 4) s	0.85p.u At (4 to 6) s
Fig. 11H	AC static load current (A)	At (0 to 1.5) s (−4. to 4.) A	At (1.5 to 4) s (−4.8 to 4.8) A	At (4 to 6) s (−4 to 4) A
Fig. 11I	AC static load voltage (V)	(−175 to 175)V	At (1.5 to 4) (−185 to 185)V	At (4 to 6) (−180 to 180)V
Fig. 11M	IM stator voltage (V)	(−370 t0 370) V		
Fig. 11N	Frequency of IM stator current (Hz)	At (0 to 2.5) s 11 Hz	At (2.5 to 6) s 8 Hz	
Fig. 11O	IM rotor speed (rad/s)	At (0 to 2.5) s 37 rad/s	At (2.5 to 6) s 24.6 rad/s	

given in Figs. 9A, 10A, 11A and 12A respectively. In addition, we note that the same behaviour occurs in the case of use generator stator current, see Figs. 9B, 10B, 11B and 12B, respectively.

For the reference and the actual load voltage, in Figs. 9G, 10G, 11G and 12G, it has been observed that the proposed control unit becomes able to track voltage with very small stabilization times while the load and rotor speed are varied.

From Figs. 9H, 11H and 12H, it is found that the value of the drawn current becomes equal to twice during the period (2–4.5) s due to the static load variations. As well as, the fuel cell produced energy is enhanced to come across the load and generates more energy while the wind generated power still constant during the interval (2–2.25) s. On the other hand, in Fig. 10H, the static load is fixed (the second case) however, varies at 1.5 to 4 s in view of the variation in the reference and actual load voltage as clarified in Fig. 10G, see also Tables 5.

From Figs. 9O, 10O, and 12O, it is clear that the IM rotor velocity reduced to 25 rad/s at a time of 2.5 s. In addition, it is observed that as the wind velocity and the load voltage varied the IM rotor velocity remains constant at its desired value. Moreover, the rotor velocity of the IM is controlled by vector control. When, the IM rotor velocity reduces, the vector control cuts down the frequency of the IM stator voltage so that the IM actual rotor velocity minimizes to its desired value. Furthermore, the performance of the proposed system as well as the suggested ANFIS controls together with vector control of the induction motor has been considered (third case) as given in Fig. 11O. Also, this case is carried out with a step change of wind velocity and static load while constant rotor velocity of the induction motor, see Table 6.

From Figs. 9A, 10A and 11A, it is obvious that the step variation of wind velocity based on the suggested neural networks (ANFIS) controller is depicted according simulation results. Moreover, when the wind speed remains constant (last case) as shown in Fig. 12A, still the proposed system can feed the static load and dynamic load with the desired value, see Table 7.

At last, the control procedure can be abbreviated as:

(a) If V_{dc} is going to increase on account of the growing in wind velocity:

The controller is turned on and the duty cycle ratio of the inverter is changed to keep V_{ac} at its recommended rate. Meanwhile, the fuel cell controller rises the charge current of the fuel cell to store any additional generated energy and keep the V_{ac} at the required

Table 6
Reactivity effect of independent wind/fuel cell supply the production constituent IM and static load through the considered control for step changes in wind velocity and static load.

Figure No.	The different Variables on y-axis	Time Variable on time-axis		
		(0–1.5) s	(1.5–4.5) s	(4.5–6) s
Fig. 12A	Wind speed (m/s)	14 m/s	11 m/s	13 m/s
Fig. 12B	SG Generator rotor speed (rad/s)	370 rpm	320 rpm	358 rpm
Fig. 12C	SG torque (Nm)	−13 Nm	−4.3 Nm	−9 Nm
Fig. 12D	SG stator current (A)	(−15 to 15) A	(−8 to 8) A	(−11.6 to 11.6) A
Fig. 12E	SG stator voltage (V)	(−370 to 370) V		
Fig. 12F	P-H2 (Pa) P-O2 (Pa)	(0.04 to 0.05) Pa (0.04 to 0.05) Pa	(0.05 to 0.06) Pa (0.05 to 0.045) Pa	(0.06 to 0.062) Pa (0.045 to 0.039) Pa
Fig. 12G	Actual & Reference load voltage (p.u)	(0.8) p.u	0.9p.u At (1.5 to 4) s	0.85p.u At (4 to 6) s
Fig. 12H	AC static load current (A)	At (0 to 1.5) s (−4. to 4.) A At (1.5 t0 2) s (−4.8 to 4.8) A	At (2 to 4) s (−9 to 9) A	At (4 to 4.5) s (−8.5 to 8.5) A At (4.5 to 6) s (−4 to 4) A
Fig. 12I	AC static load voltage (V)	(−175 to 175)V	(−182 to 182)V	
Fig. 12M	IM stator voltage (V)	(−370 t0 370) V		
Fig. 12N	Frequency of IM stator current (Hz)	11 Hz		
Fig. 12O	IM rotor speed (rad/s)	At (0 to 6) s 37 rad/s		

Table 7
Reactivity effect of independent wind/fuel cell supply the production constituent IM and static load through the considered control for step changes in wind velocity and static load.

Figure No.	The different Variables on y-axis	Time Variable on time-axis		
		(0–1.5) s	(1.5–4.5) s	(4.5–6) s
Fig. 13A	Wind speed (m/s)	12 m/s		
Fig. 13B	SG rotor speed (rad/s)	370 rpm		
Fig. 13C	SG torque (Nm)	−7 Nm		
Fig. 13D	SG stator current (A)	(−8 to 8) A		
Fig. 13E	SG stator voltage (V)	(−370 to 370) V		
Fig. 13F	P-H2 (Pa) P-O2 (Pa)	(0.04 to 0.05) Pa (0.04 to 0.05) Pa	(0.05 to 0.06) Pa (0.05 to 0.045) Pa	(0.06 to 0.062) Pa (0.045 to 0.039) Pa
Fig. 13G	Actual & Reference load voltage (p.u)	(0.8) p.u	0.9p.u At (1.5 to 4) s	0.85p.u At (4 to 6) s
Fig. 13H	AC static load current (A)	At (0 to 1.5) s (−4. to 4.) A At (1.5 to 2) s (−4.8 to 4.8) A	At (2 to 4) s (−9 to 9) A	At (4 to 4.5) s (−8.5 to 8.5) At (4.5 to 6) s (−4 to 4) A
Fig. 13I	AC static load voltage (V)	(−175 to 175)V	(−182 to 182)V	
Fig. 13M	IM stator voltage (V)	(−370 to 370) V		
Fig. 13N	Frequency of IM stator current (Hz)	At (0 to 2.5) s 11 Hz	At (2.5 to 6) s 8 Hz	
Fig. 13O	IM rotor speed (rad/s)	At (0 to 2.5) s 37 rad/s	At (2.5 to 6) s 25 rad/s	

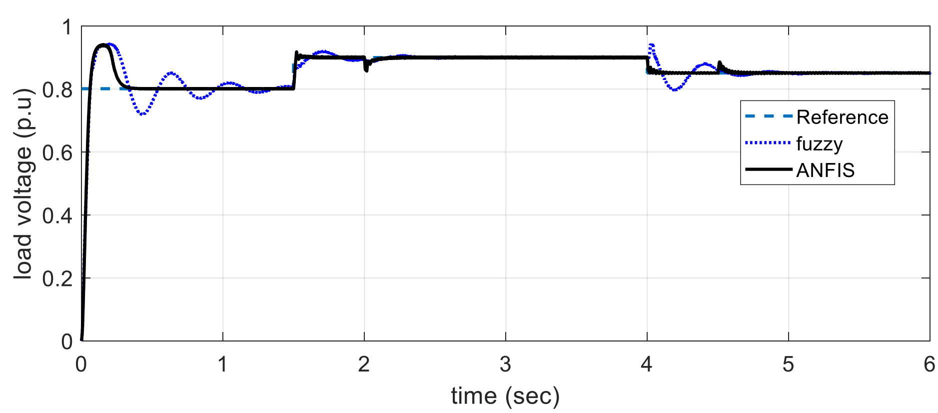

Fig. 13. Reference and actual load voltage based on the proposed ANFIS and fuzzy controls of autonomous wind/fuel cell providing IM and static load step changes in velocity of the IM and static load.

Table 9
Parameters and Data of the proposed system.

IM-squared –cage
3 phase, 20 HP, 460 V, 60 Hz, 1760 rpm, 2 poles
$R_s = 0.27614\Omega$
$L_d = 2.19\mu$ H
$L_q = 76.14\mu$ H
$J = 0.1kgm^2$
Wind turbine, Rating: 1 kw, 450 rpm (low speed side) at = 12 m/s
Equator radius (R) = 1 m
Swept area (A) = 4 m^2
ρ = 1.25 kg/m^3

Table 10
Fuel cell system data [23].

Symbol	Value	Parameter	Unit
E_r	1.189	Reference potential	V
R	8.314	Ideal gas constant	J/mol.K
F	96,485	Faraday's constant	C
T_k	333	Temperature In Kelvin	K
i_{loss}	0.002	Lost in Current	A cm^{-2}
i_o	3×10^{-6}	Exchange current density	A cm^{-2}
i_l	1.6	Limiting current density	A cm^{-2}
R_i	0.15	Internal Resistance	Ohm- cm^2
P_{H_2}	3	Hydrogen pressure	Pa
P_{air}	3	Air pressure	Pa
P	1.2	Cell pressure	Pa
G	228,170	Gibbs free energy	J/mol
T_c	60	Temperature in degrees	C
A	100	Area of cell	Cm^2
k	1.1	Constant k used in mass transport	
α_t	1	Transfer coefficient	
n	2	Number of Cells	

Table 11
Abbreviations.

Symbol	Definition
ANFIS	Adaptive Neuro Fuzzy Inference System
BLDC	Brushless **DC**
C_p	Power Coefficient.
$C_{p_{max}}$	Maximum Power Coefficient
C_T	Wind Turbine Torque Coefficient.
DFIG	Doubly fed induction generator
DG	Distributed generator
DVR	Dynamic voltage restorer
FC	Fuel Cell
G	Gibbs Free Energy
HPS	Hybrid power system
HRES	Hybrid renewable energy systems
IM	Induction Motor.
i_{sd}, i_{sq}	d-q Stator Currents of PMSG.
i_{ds}, i_{qs}	d-q Stator Currents of IM.
$I_{Dc(rect.)}$	Rectifier Output Current.
L_{sd}	Stator Inductance at d-axis
L_{sq}	Stator Inductance at q -axis
MOSSA	Multi-Objective Salp Swarm Algorithm
MPPT	Maximum Power Point Tracking
P_m	Wind Power.
PEMFC	Proton exchange membrane fuel cell
PI	Proportional-integral
PMSG	Permanent Magnet Synchronous Generator
PV	Photovoltaic
QMLI	Quinary multilevel inverter
SG	Synchronous Generator
THD	Total harmonic distortion
TSBC	Two switches boost converter
TSR	Tip Speed Ratio
UPFC	Unified power flow controller
v_{sd}, v_{sq}	d-q Stator Voltages of the PMSG.
v_{sd}, v_{sq}	d-q Stator Voltages of the IM.
$V_{Dc(rect.)}$	Rectifier Output Voltage.
WECS	Wind energy conversion system
WTG	Wind Turbine Generator

rate. Consequently, the generator and voltage going to minimize until stabilized to the convenient value. The vector control regulates the IM stator voltage until the IM rotor velocity reaches its recommended value. If the DC-link voltage attempts to minimize on account of the low wind velocity, the controllers will implement an action which is counteractive to that outlined above as illustrated in Figs. 9, 10, 11 and 12.

(b) When the IM reference rotor velocity is reduced, the IM rotor velocity is minimized to supersede its recommended value by diminishing the motor stator frequency.

(c) The use of a storage fuel cell helps maintain a DC voltage to be stable in the event of wind and/or load changes.

Finally, the outcomes that obtained according to the suggested ANFIS controller are compared with the same results as when applying classical fuzzy controller as represented in Fig. 13. It is noticed that the reference voltage equals 0.8 p.u. at starting, while the actual voltage started at zero value and tracked the reference value. Therefore, the obtained results based on ANFIS are better than in case of applying classical fuzzy control in the settling time. Whereas, as shown in this Fig. 13, Fuzzy Control took about 4.5 s. to reach stability time, unlike ANFIS control, as it did not take long to reach stability time as presented in Figs. 9–12G.

6. Conclusions

Generally, this paper deals with power optimization strategy used in the wind turbine power system as well as wind system and energy storage which used to store energy and to reduce the output power fluctuation. In more details, it presents a control strategy for hybrid wind/fuel cell energy system providing static and dynamic loads during DC/AC converter, induction motor (IM) as a dynamic load and water electrolizer for supplying hydrogen gas in the context of artificial intelligence techniques. To ensure efficient optimization of sources, ANFIS strategy is employed to achieve a stable and dynamic load as well as to recompense the reduction in wind power and/or share the extra needed power from the load. Furthermore, it is illustrated in the mathematical models of the system for wind turbines, calculating the MPPT values for some of the different important cases as well as finding the

Table 8
Constant parameters of turbine blade [21].

Constant parameters c_i	c_1	c_2	c_3	c_4	c_5	c_6	c_7	c_8
Value	0.5	116	0.4	0	2	5	21	0.08

Table 12
Nomenclature.

Symbol	Unit	Definition
A	m^2	Blade swept area
E	V	Cell Potential
F	$Cmol^{-1}$	Faraday's constant
i	A/m^2	Output current density
I_g	A/m^2	Current Phase of the PMSG
i_o	A/m^2	Exchange current density
i_L	A/m^2	Limiting current density
i_{loss}	A/m^2	Current loss
P_{H_2O}	Pa	Saturation pressure of water
P_{H_2}	Pa	Hydrogen partial pressure
P_{O2}	Pa	Oxygen partial pressure
r	m	Rotor radius
R	$Jmol^{-1}K^{-1}$	Universal gas constant
R_i	Ωm^2	Internal resistance
T	K	Operating temperature
T_k	K	Fuel cell temperature
T_m	N.m	Wind turbine torque
V_{act}	V	Activation over-voltage
V_{con}	V	Concentration over-voltage
V_{fc}	V	Fuel cell potential
V_g	V	Phase voltage of the PMSG terminal
V_{ohm}	V	Ohmic over-voltage
V_{ω}	m/s	Wind speed
Greek symbols		
α		Change transfer coefficient
β		Blade Pitch angle
ρ	kg/m^3	Air density
μ		Parameter depends on λ and β (in (3) and (4))
λ		Tip speed ratio
λ_m	$kg.m^2s^{-2}A^{-1}$	Flux linkage the PMSG
λ_{opt}		Optimum tip speed ratio
ω_t	rad/s	Angular rotor speed of the turbine rotor
ω_r	rad/s	Angular rotor speed of the PMSG

mathematical formulas for PMSG and PEM model. Some useful and required calculations are shown graphically. The whole system is analysed through simulation in MATLAB/Simulink environment.

So, the following can be summarized:

- The considered hybrid wind/fuel cell generation system is capable of supplying static and dynamic loads.
- The fuel cell generator unit works to recompense for the decreasing in wind power and/or the increasing power required by the loads.
- The chosen controller unit is qualified to follow recommended load energy through a small settling time and small maximum overshoot.
- The suggested control unit can conserve the load voltage at its required recommended value of any differences in the velocity of the wind and/or changes in variables of dynamic and static loads.
- It is noted that the performance of the studied system is better than in case of applying the classical fuzzy control especially in case of transient response.
- Finally, it is found that the results that obtained by the suggested ANFIS control model for the hybrid system gives a greater reliability in terms of power generation and distribution compared to classical fuzzy control.

Declaration of Competing Interest

The authors declare that they have no known competing financial interests or personal relationships that could have appeared to influence the work reported in this paper.

Appendix A

See Tables 8–12.

References

[1] Senjyu T, Tamaki S, Muhando E, Urasaki N, Kinjo H, Funabashi T, et al. Wind velocity and rotor position sensorless maximum power point tracking control for wind generation system. Renewable Energy 2006;31(11):1764–75.
[2] Rajkumar RK, Ramachandaramurthy VK, Yong BL, Chia DB. Techno-economical optimization of hybrid pv/wind/battery system using Neuro-Fuzzy. Energy 2011;36(8):5148–53. doi: https://doi.org/10.1016/j.energy.2011.06.017.
[3] Mendis N, Muttaqi KM, Sayeef S, Perera S. Standalone operation of wind turbine-based variable speed generators with maximum power extraction capability. IEEE Trans Energy Convers 2012;27(4):822–34.
[4] Atawi IE, Kassem AM, Zaid SA. Modeling, management, and control of an autonomous wind/fuel cell micro-grid system. Processes 2019;7(2):85.
[5] Hassan AA, Kassem AM. Modeling, simulation and performance improvements of a PMSM based on functional model predictive control. Arab J Sci Eng 2013;38(11):3071–9. doi: https://doi.org/10.1007/s13369-012-0460-6.
[6] Atawi I, Kassem AM. Optimal control based on maximum power point tracking (MPPT) of an autonomous hybrid photovoltaic/storage system in micro grid applications. Energies 2017;10(5):643.
[7] Fathy A, Kassem AM, Abdelaziz AY. Optimal design of fuzzy PID controller for deregulated LFC of multi-area power system via mine blast algorithm. Neural Comput Appl 2020;32(9):4531–51.
[8] Kassem AM. Modeling and robust control design of a stand-alone wind- based energy storage generation unit powering an induction motor variable-displacement pressure compensated pump'. IET Renew Power Gener 2016;10(3):275–86.
[9] Kumar V, Joshi RR. Development of a novel control for a matrix converter interfaced wind energy conversions system for dynamic performance enhancement. J Electric Power Comp Syst 2015;43(8):1062–71.
[10] Abdalla SA, Abdullah SS. Performance improvements of induction motor drive supplied by hybrid wind and storage generation system based on mine blast algorithm. Energies 2019;12(15):2947. doi: https://doi.org/10.3390/en12152947.
[11] Murugesan K, Subramaniam U. Characterization and experimental validation of a semi-empirical fuel cell model for investigating the water dynamics on the electrical behavior of a 5 kW Ballard stack system using Nafion 117 polymer membrane. J Renew Sustain Energy 2020;12(2):024301. doi: https://doi.org/10.1063/1.5121609.
[12] Vuppala RK, Chaedir BA, Jiang L, Chen L, Aziz M, Sasmito AP. Optimization of membrane electrode assembly of PEM fuel cell by response surface method. Molecules 2019;24:3097. doi: https://doi.org/10.3390/molecules24173097.
[13] Tijani AS, Binti Kamarudin NA, Binti Mazlan FA. Investigation of the effect of charge transfer coefficient (CTC) on the operating voltage of polymer electrolyte membrane (PEM) electrolyzer. Int J Hydrogen Energy 2018;43(19):9119–32.
[14] Chang-Chien L-R, Sun C-C, Yeh Y-J. Modeling of wind farm participation in AGC. IEEE Trans Power Syst 2014;29(3):1204–11.
[15] Wilk A, Węcel D, Mohamad A, Taler J, Benim AC, Bennacer R, et al. Analysis of the Proton Exchange Membrane Fuel Cell in transient operation. E3S Web of Conferences 2019;128:01026. doi: https://doi.org/10.1051/e3sconf/201912801026.
[16] Lamus RL, Raël S, Berger K, Hinaje M, Lévêque J. PEM single fuel cell as a dedicated power source for high-inductive superconducting coils. Int J Hydrogen Energy 2018;43(11):5913–21. doi: https://doi.org/10.1016/j.ijhydene.2017.09.013ff.ffhal-01584823ff.
[17] Martín IS, Ursúa A, Sanchis P. Modelling of PEM fuel cell performance: steady-state and dynamic experimental validation. Energies 2014;7:670–700. doi: https://doi.org/10.3390/en7020670.
[18] Rezzak D, Khoucha F, Benbouzid MEH, Kheloui A, Mamoune A. A DC-DC converter-based PEM fuel cell system emulator. In: Proceedings of the 2011 International Conference on Power Engineering, Energy and Electrical Drives Torremolinos (Málaga), Spain. May; 2011.
[19] Fathy A, Kassem AM. Antlion optimizer-ANFIS load frequency control for multi-interconnected plants comprising photovoltaic and wind turbine. ISA Trans 2019;87:282–96.
[20] Eshetu W, Sharma P, Sharma C. ANFIS based load frequency control in an isolated micro grid. In: 2018 IEEE International Conference on Industrial Technology (ICIT), Lyon; 2018. p. 1165–70.
[21] Hossain M, Mekhilef S, Afifi F, Halabi LM, Olatomiwa L, Seyedmahmoudian M, et al. Application of the hybrid ANFIS models for long term wind power density prediction with extrapolation capability. PLoS ONE 2018;13(4):e0193772. doi: https://doi.org/10.1371/journal.pone.019377210.1371/journal.pone.0193772.g00110.1371/journal.pone.0193772.g00210.1371/journal.pone.0193772.g00310.1371/journal.pone.0193772.g00410.1371/journal.pone.0193772.g00510.1371/journal.pone.0193772.g00610.1371/journal.pone.0193772.g00710.1371/journal.pone.0193772.g00810.1371/journal.pone.0193772.g00910.1371/journal.pone.0193772.g01010.1371/journal.pone.0193772.g01110.1371/journal.pone.0193772.g01210.1371/journal.pone.0193772.

g01310.1371/journal.pone.0193772.g01410.1371/journal.pone.0193772.g01510.1371/journal.pone.0193772.g01610.1371/journal.pone.0193772.g01710.1371/journal.pone.0193772.g01810.1371/journal.pone.0193772.g01910.1371/journal.pone.0193772.g02010.1371/journal.pone.0193772.g02110.1371/journal.pone.0193772.t00110.1371/journal.pone.0193772.t00210.1371/journal.pone.0193772.t00310.1371/journal.pone.0193772.t00410.1371/journal.pone.0193772.t00510.1371/journal.pone.0193772.t00610.1371/journal.pone.0193772.t00710.1371/journal.pone.0193772.t00810.1371/journal.pone.0193772.t00910.1371/journal.pone.0193772.t01010.1371/journal.pone.0193772.t01110.1371/journal.pone.0193772.t01210.1371/journal.pone.0193772.s001.

[22] Kanagasakthivel B, Devaraj D, Banu RN, Selvi VI. A hybrid wind and solar energy system with ANFIS based MPPT controller. J Intelligent Fuzzy Syst 2018;35(3):1–17.

[23] Garcia P, Garcia CA, Fernandez LM, Llorens F, Jurado F. ANFIS-based control of a grid-connected hybrid system integrating renewable energies, hydrogen and batteries. IEEE Trans Ind Inf 2014;10(2):1107–17. doi: https://doi.org/10.1109/TII.2013.2290069.

[24] Neelima V, Hameed S, Jyothi M. ANFIS strategy for wind/fuel cell power management system in a microgrid. Int J Emerg Trends Electrical Electron 2014;10(9):1–11.

[25] Amin IK, Nasir Uddin M, Marsadek M. ANFIS based neuro-fuzzy control of DFIG for wind power generation in standalone mode. In: 2019 IEEE International Electric Machines Drives Conference (IEMDC); 2019. p. 2077–82. https://doi.org/10.1109/IEMDC.2019.8785334.

[26] Falehi AD, Rafiee M. Optimal control of novel fuel cell-based DVR using ANFISC-MOSSA to increase FRT capability of DFIG-wind turbine. Soft Comput 2019;23:6633–55. doi: https://doi.org/10.1007/s00500-018-3312-9.

[27] Jurado F, Ortega M, Carpio J. Power quality enhancement in fuel cells using genetic algorithms and ANFIS architecture. In: 2006 IEEE International Symposium on Industrial Electronics; 2006. p. 757–62. https://doi.org/10.1109/ISIE.2006.295729.

[28] Mohanty A, Viswavandya M, Mishra D, Ray P, Mohanty SP. ANFIS based sliding mode controller for reactive power compensation in fuel cell based hybrid power system. In: 2016 International Conference on Signal Processing, Communication, Power and Embedded System (SCOPES); 2016. p. 851–5. https://doi.org/10.1109/SCOPES. 2016.7955562.

[29] Reddy KJ, Sudhakar N. ANFIS-MPPT control algorithm for a PEMFC system used in electric vehicle applications. Int J Hydrogen Energy 2019;44(29):15355–69. doi: https://doi.org/10.1016/j.ijhydene.2019.04.054.

[30] Nazar AA, Jayabharath R, Udayakumar MD. An ANFIS based advanced MPPT control of a wind-solar hybrid power generation system. IREMOS 2014;7:638. https://doi.org/10.15866/iremos.v7i4.2457.

[31] Subha S, Nagalakshmi S. Design of ANFIS controller for intelligent energy management in smart grid applications. J Ambient Intell Human Comput 2021;12(6):6117–27. doi: https://doi.org/10.1007/s12652-020-02180-y.

[32] Thirumalaisamy B, Jegannathan K. A novel energy management scheme using ANFIS for independent microgrid. Int J Renew Energy Res (IJRER) 2016;6:735–46.

[33] Khare V, Khare C, Nema S, Baredar P. Tidal energy systems, design. Optimization and control, Ch 5 - Control system of tidal power plant; 2019. p. 243–94, https://doi.org/10.1016/B978-0-12-814881-5.00005.

[34] Dicks AL, Rand DAJ, editors. Fuel cell systems explained. Wiley; 2018.

[35] Woonki BG, Diong NB. Linear and nonlinear models of fuel cell dynamics from: fuel cells: dynamic modeling and control with power electronics applications. CRC Press; 2016. https://doi.org/10.1201/9781315369860-4.

[36] Barbir F. PEM fuel cells: theory and practice. second ed. Academic Press; 2013.

[37] Spiegel C. PEM fuel cell modelling and simulation using MATLAB. Oxford UK: Elsevier Academic Press; 2008.

[38] Jang JSR, Sun CT, Mizutani E. Neuro-fuzzy and soft computing: a computational approach to learning and machine intelligence. Prentice Hall Inc.; 1997.

[39] Jang JSR, Sun CT. Neuro-fuzzy modeling and control. Proc IEEE 1995;83(3):378–406.

[40] Priyadarshi N, Padmanaban S, Holm-Nielsen JB, Blaabjerg F, Bhaskar MS. An experimental estimation of hybrid ANFIS-PSO-based MPPT for PV grid integration under fluctuating sun irradiance. IEEE Syst J 2020;14(1):1218–29. doi: https://doi.org/10.1109/JSYST.2019.2949083.

[41] Priyadarshi N, Padmanaban S, Bhaskar MS, Blaabjerg F, Holm-Nielsen JB, Azam F, et al. A hybrid photovoltaic-fuel cell-based single-stage grid integration with lyapunov control scheme. IEEE Syst J 2020;14(3):3334–42. doi: https://doi.org/10.1109/JSYST.2019.2948899.